Chapter 9 Capillary Adhesion of Mico-beams and Plates: A Review

Jian-lin Liu[1] and Re Xia[2]

[1] *Department of Engineering Mechanics, China University of Petroleum, Qingdao 266555, China*
[2] *Schoool of Power and Mechanical Engineering, Wuhan University, Wuhan 430072, China*

Abstract: A review is presented for the capillary adhesion of micro-beams and plates, and this phenomenon exists widely in MEMS, animal hairs, carbon nanotubes or nanowires. Although the capillary force is usually negligible at the macroscopic scale of human buildings, bridges or vehicles, it becomes dominant at small scales since the surface/volume ratio increases as smaller objects are considered. In this review, we show the fundamental theory and analysis method for general problems of capillary adhesion. Firstly, for the adhesion of micro-beam or micro-plate, the existing investigation deals with the cases of both infinitesimal and finite deformation. In use of the principle of minimum total potential energy, the critical adhered length and deflection of the micro-structure can be derived. Furthermore, the mechanism of the hierarchical structure in adhesion can be elucidated by means of energy theory. The method adopted in this chapter can also be developed to solve other adhesion problems associated with van der Waals force or electrostatic force. These findings may provide inspirations for the design of micro-devices, MEMS, micro-sensor and non-wetting materials from different aspects (e.g., geometric shape, characteristic size, surface microstructure and elasticity).

Keywords:

9.1 Introduction

Capillary action of liquid exists widely in nature, which causes a lot of interesting phenomena in industry and our daily life. For example, water can be transported by capillary tubes in plants, the lotus and lady's mantle have the strong capability of self-cleaning, i.e."lotus effect"[1-3], water striders or spiders can walk or jump freely on water surface[4,5], Texas horned lizard draws water by capillary action through thin channels that extend from its feet to mouth[6], some millimeter-scale water-walking insects can arrive at

the land with the help of a lateral capillary force originating from the meniscus surface[7], shore birds can remove a liquid drop with its beak opening and closing in a tweezering motion[8], and the solid components floating at liquid interfaces can self-assemble automatically by their interacting forces[9]. Additionally, capillary force or surface tension is closely related to various applications in industry, e.g., porous media, micro-fluidic devices, self-cleaning paints, and glass windows[10,11].

Another important issue about surface tension is the capillary adhesion of micro-structures or devices. In the past decades, wide attention has been attracted on the adhesion of materials and devices at micro- and nano-scales, which may be caused by van der Waals force, Casimir force, capillary force or some other interaction forces[12-15]. On one hand, adhesion may cause the failure or collapse of micro-electromechanical systems (MEMS)[12]. In microcontact printing technology, for instance, adhesion associated with van der Waals force leads to stamp deformation and limits the application of this technology[16,17]. Three kinds of stamp deformation, i.e., roof collapse, buckling and lateral sticking of the fibrillar structures, have been observed in the process. Besides, van der Waals force may also cause the stiction of high aspect ratio SU-8 resist when preparing the photonic crystals. On the other hand, adhesion mechanisms may be useful in the manipulation and operation of some micro-devices, which are also beneficial for various biological processes of creatures, such as adhesion of biological macromolecules, cells or vesicles on a substrate[18-20]. Among others, an interesting example is the striking adhesion ability of gecko, which is attributed primarily to the van der Waals force between their feet and the contact surfaces[21,22].

In the process of adhesion, hierarchical structure may often appear compared with some other morphologies. In fact, structural hierarchy plays a significant role in the physical properties and biological behavior of various kinds of man-made and natural materials and systems (e.g., the branches and roots of trees, and the hierarchical macro/meso/micro/nano structure of bones, silks and other biomaterials). As a representative example, the hierarchical structures of the specialized adhesive feet of geckos attracted great interest in the past few years. Gao et al.[23,24] used the fractal concept to characterize the self-similar fibrillar structures of gecko feet at multiple levels, and elucidated the importance of the nanometer length scale and structural hierarchy on the superior adhesion strength.

In this review, we focus on the adhesion of micro-structures induced mainly by capillary force of liquid films/bridges. In the areas of biology surface, carbon nanotube (CNT) array, MEMS, micro-sensor and micro-fluidics, surface tension or capillary force becomes a predominant factor with the ratio of surface and volume increasing. Capillary adhesion may often happen in the fast developing MEMS techniques, in which typical surface separations are in the range of 500 – 2000 nm. Henceforth, water can be trapping in the gaps of the high surface tension micromachining structures and then produce strong capillary forces[12,25]. The capillary force may even drive the CNT ar-

rays to reorganize into cellular structure upon drying and produce different nano-patterns of CNT arrays on thin films[26,27]. The process of self-assembly of ZnO nanowire arrays into hierarchical patterns is also driven by the capillary force[28]. What is more, the adhesion of animal hairs, carbon nanotubes or nanowires of a periodically or randomly distributed array always leads to hierarchical structures[29]. As yet, however, there is a lack of theoretical investigation on why and how hierarchical structures form due to adhesion.

Therefore, the outline of this chapter is planned as follows: First, we will mention the capillary adhesion models of micro-beams of infinitesimal deformation. Then the finite deformation of micro-beams induced by surface tension will be introduced. Next, the mechanism of the hierarchical structure of two bundles of beams will be presented. Finally, some other capillary adhesion phenomena about plates will be reviewed.

9.2 Capillary adhesion of micro-beams of infinitesimal deformation

For the characteristic size of MEMS has been reduced to micro or nano-meter, capillary force is considered as a dominant factor in design and fabricate. To avoid the collapse of capillary adhesion of MEMS structures, a lot of experimental and analytical models have been analyzed and constructed. For example, Mastrangelo et al.[14,15] analyzed the deflection, mechanical stability and adhesion of thin micromechanical structures under capillary forces. They got an approximate condition to avoid adhesion contact of a structure to the substrate. Zhu et al.[30] also investigated the adhesion of microcantilevers driven by the capillary force and calculated the critical values of surface energy for initial and full adhesion of two opposing cantilevers. De Bohr[31] calculated the characteristic parameters of a beam adhered by liquid on a rough substrate, and compared them with the experimental results. By using the fracture mechanics theory, they pointed out that the work of adhesion is equal to the surface energy difference in the separated versus the joined materials minus an interfacial energy term. Their analysis includes the evaporation of liquid at the interface between two solid materials.

Li et al.[32] also carried out an experiment to study the deflection of a cantilever adhered by a liquid bridge using electronic speckle pattern interferometry (ESPI). They measured the transient deformation of a microcantilever caused by the capillary force, and then constructed the energy function of the adhesion system based on the independent parameters of adhesion length and volume fraction of the adhesion medium. The experimental result of the cantilever in equilibrium is consistent with the analytical solution. Moreover, Kwon et al.[33] analyzed the spontaneous spreading of a liquid drop confined between an elastic plate and a rigid substrate due to the effects of interfacial forces. The eventual equilibrium shape of the droplet is determined by the

balance between elastic and capillary effects. They provided an analytical theory for the static shape of the sheet and the extent of liquid spreading, and the result shows that the experiments are quantitatively consistent with the theory. The theory is relevant to the first step of painting when a brush is brought down onto canvas. More mundanely, the result allows us to understand the stiction of microcantilevers to wafer substrates occurring in microelectromechanical fabrication processes.

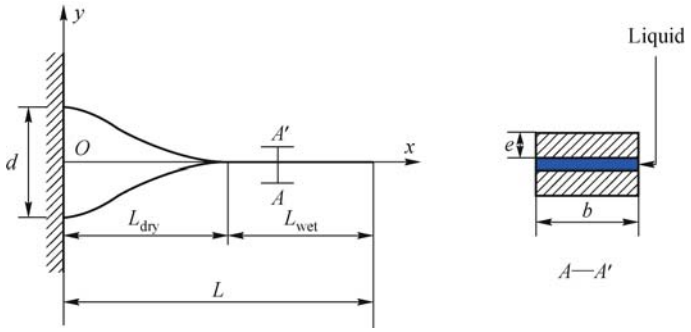

Fig. 9.1 Capillary adhesion of two micro-beams of infinitesimal deformation.

Recently, Bico et al., Kim, Mahadevan and Liu et al.[29,34,35] calculated the critical dry length of two or two bundles of adhered hairs by considering capillary force and elastic deformation. Refer to a Cartesian coordinate system $(O-xy)$. For two micro-beams adhered by a thin liquid film, as shown in Fig.9.1, the hairs are assumed to have an identical size of length L,width b, and thickness e. The distance between the two hairs at the clamped ends is d. The lengths of the dry (unadhered) and the wet (adhered) segments are denoted as $L_{\rm dry}$ and $L_{\rm wet}$, respectively. The deflections of the two beams are symmetric with respect to x-axis. The deflection of the upper beam can be written as

$$w = \frac{d}{L_{\rm dry}^3}x^3 - \frac{3d}{2L_{\rm dry}^2}x^2 + \frac{d}{2} \tag{9.1}$$

according to the boundary conditions: $w(0) = d/2, w'(0) = 0$, $w(L_{\rm dry}) = 0$, and $w'(L_{\rm dry}) = 0$. The total potential energy includes two parts, namely, the strain energy and the surface energy, which can be expressed as

$$\begin{aligned} \Pi &= \frac{EI}{2}\int_0^{L_{\rm dry}} (w'')^2 {\rm d}x + 2(\gamma_{\rm SL} - \gamma_{\rm SV})L_{\rm wet}b \\ &= \frac{3EId^2}{L_{\rm dry}^3} - 2\gamma\cos\theta_{\rm Y}(L - L_{\rm dry})b, \end{aligned} \tag{9.2}$$

where E is the Young's modulus, $I = be^3/12$ the inertia moment of the beam, and w the deflection. The symbols $\gamma_{\rm SL}$ and $\gamma_{\rm SV}$ denote the surface tension of solid/liquid and solid/vapor interfaces, respectively, which satisfy

the Young's equation, $\gamma_{SV} - \gamma_{SL} = \gamma \cos\theta_Y$, with γ being the surface tension of liquid/vapor interface and θ_Y being the Young's contact angle of the beam.

In use of the principle of minimum total potential energy, one can obtain the critical length in equilibrium state according to the condition of $\dfrac{\mathrm{d}\Pi}{\mathrm{d}L_{\mathrm{dry}}} = 0$:

$$L_{\mathrm{dry}} = \sqrt[4]{\frac{3Ee^3d^2}{8\gamma\cos\theta_Y}}. \tag{9.3}$$

The analytical result of Eq.(9.3) is compared with Liu's experimental result in Fig.9.2, which indicates that this solution is in good agreement with the actual case. Furthermore, we can see that if the total length $L < L_{\mathrm{dry}}$, the adhesion energy induced by the introduction of a liquid film between the two beams is insufficient to provide the strain energy of deformation, and therefore, the two beams will not adhere together. On the contrary, if $L > L_{\mathrm{dry}}$, the surface energy is higher than the strain energy, and then the adhesion of the two beams becomes possible. The calculated result requires that the contact angle θ_Y must satisfy $0 \leqslant \theta_Y < \pi/2$, that is, the hairs must be hydrophilic. In other words, capillary adhesion can not happen between two hydrophobic hairs.

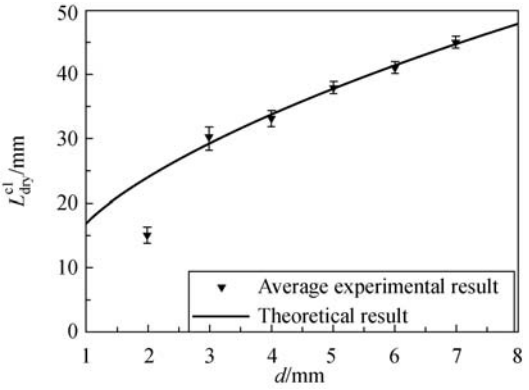

Fig. 9.2 Critical adhesion length as a function of the spacing of two micro-beams.

Based upon the similar analysis, Liu et al.[35] investigated the capillary adhesion of three beams and two bundles of beams, and got the similar results. Also, this method applies to the capillary adhesion of a beam stuck on a solid substrate.

9.3 Capillary adhesion of micro-beams of finite deformation

The above analyses of capillary adhesion in Section 9.2 are mainly based on the elastic theory of a beam in small deformation. However, the deformation of the adhered CNTs and micro-beams is often large because of their very small bending stiffness. The infinitesimal deformation approximation may cause a significant error in the solutions. Therefore, based upon the experimental phenomenon of Journet et al.[36], Liu et al.[37] constructed the adhesion models of two beams which were adhered by the capillary force in finite deformation, as shown in Fig.9.3a. The beams are modeled as two parallel cantilevers of length L, whose right ends are clamped with a distance d in between. Without loss of generality, the beams are assumed to have an identical circular cross-section of radius R and that their left segments of length l are adhered by water or other liquids. Refer to the Cartesian coordinate system $(O-xy)$. Besides the Euler coordinate x, the arc length s, which is a Lagrange coordinate, is also used in the analysis. Because of the configurational symmetry, only the upper beam will be considered. For simplicity, the constraints at its right end are released and, instead, a force P and a moment M as yet to be determined are applied there, as shown in Fig.9.3b. The slope angle of the beam at point s is denoted by a function $\phi(s)$, with $\phi(l_0) = \phi_0$ at the midpoint $s = l_0 = (L + l)/2$ of the dry segment. Assuming that the beam is inextensible, the boundary conditions are $\phi(l) = 0, y(l) = 0, \phi(L) = 0$ and $y(L) = d/2$. In addition, the configurational symmetry requires that $\dot{\phi}(l_0) = 0$ and $y(l_0) = d/4 = y(L)/2$ at the midpoint

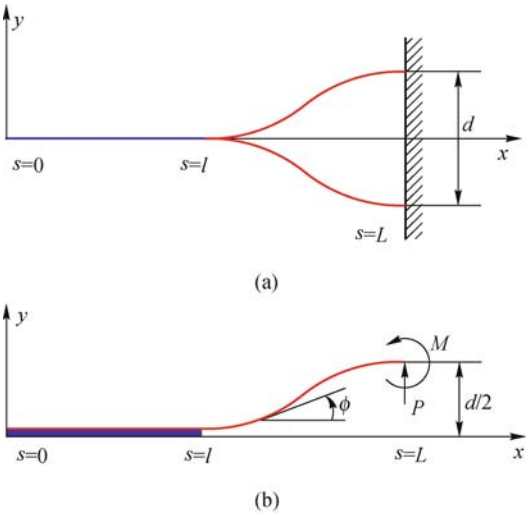

Fig. 9.3 Capillary adhesion of two micro-beams of finite deformation.

$s = l_0$ of the dry segment, where the dot symbol stands for the derivation with respect to s.

The total potential energy of the system contains the elastic strain energy, the surface/interface energy and the potential energy of the external forces. Considering the geometrical relation $\dot{y} = \sin\phi$, the energy functional with respect to the deflection of the beam is expressed as

$$\Pi = \int_l^{l_0} EI\dot{\phi}^2 \mathrm{d}s + (\gamma_{\mathrm{SL}} - \gamma_{\mathrm{SV}})bl - 2Py(l_0) + \int_l^{l_0} \lambda(\dot{y} - \sin\phi)\mathrm{d}s, \quad (9.4)$$

where $\lambda(s)$ is a Lagrange multiplier, and $I = \pi R^4/4$ the inertial moment of the beam of a solid cylindrical cross-section. The width of the liquid film between the two beams is assumed to be $b = \pi R$. In the above analysis, the strain of the linearly elastic beam is still assumed to be infinitesimal though large displacement and nonlinear force-deflection relationship are considered. This assumption is usually reasonable for slender beams.

The variation of the functional in Eq.(9.4) about the real deflection curve of the beam should equal zero, that is, $\delta\Pi = 0$. Then, one may derive the governing equation named as Euler-Lagrange equation

$$\ddot{\phi} + \alpha^2 \cos\phi = 0, \quad (9.5)$$

where $\alpha^2 = P/(EI)$. The transversality boundary condition at $s = l$ can also be derived as $\dot{\phi}(l)^2 = \gamma\cos\theta_{\mathrm{Y}} b/(EI)$, corresponding to the balance between surface/interface energy and elastic strain energy.

Using the inextensible condition of the beam, the deflection at $s = l_0$ is derived as

$$\frac{d}{4} = (l_0 - l)\left[1 - 2\frac{E(k) - E(k,\theta_1)}{F(k) - F(k,\theta_1)}\right], \quad (9.6)$$

where $\sin\theta_1 = \dfrac{1}{\sqrt{2}k}$, $F(k)$ and $F(k,\theta_1)$ are the complete and the incomplete elliptic integrals of the first kinds, and $E(k)$ and $E(k,\theta_1)$ the second kinds, respectively. From Eq.9.6 in conjunction with the transversality condition $\alpha = \sqrt{\dfrac{\gamma\cos\theta_{\mathrm{Y}} b}{2EI\sin\phi_0}}$, the values of k and l can be determined for a given d. Thereby, the other parameters ϕ_0, l_0, α, P and M can also be solved.

Then from Eq.(9.6), the deflection of the beam can be calculated from the finite deformation analysis. The Cartesian coordinates of an arbitrary point of the deformed beam can be given by

$$\begin{cases} \alpha x = \alpha l + 2k(\cos\theta_1 - \cos\theta) \\ \alpha y = \displaystyle\int_{\theta_1}^{\theta} \frac{2k^2\sin^2\theta - 1}{\sqrt{1 - k^2\sin^2\theta}}\mathrm{d}\theta. \end{cases} \quad (9.7)$$

According to the above equations, the deflection curves of the two adhered CNTs predicted by the two methods are plotted in Fig.9.4 for a representative

distance d=500 nm. For a beam with large displacement, the deformation predicted by finite deformation theory seems to be more "stiffer" than that predicted by infinitesimal deformation analysis. The considerable difference between the results of the two methods clearly evidences the necessity of adopting the finite deformation elasticity theory to analyze microsized and nanosized beams.

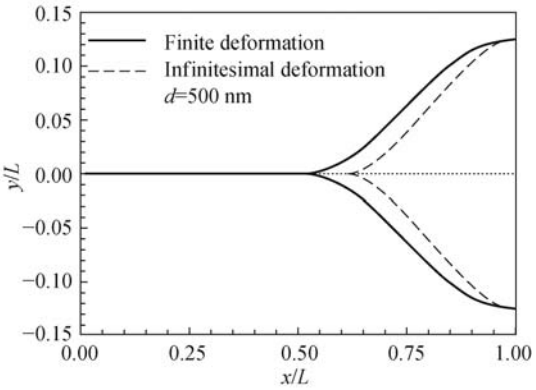

Fig. 9.4 The deflections of two micro-beams adhered by a liquid film in infinitesimal or finite deformation.

Seeing the elliptical integration solution of Eq.(9.7), Liu[38] found that there is an interesting analogy between a liquid bridge and a cantilever of finite deformation, as shown in Figs.9.5 and 9.6. It indicates that the two governing equations take the same style after coordinate translation and scale transformation. The stiffness, generalized force, curvature, energy origination and some other parameters are compared for the two physical phenomena

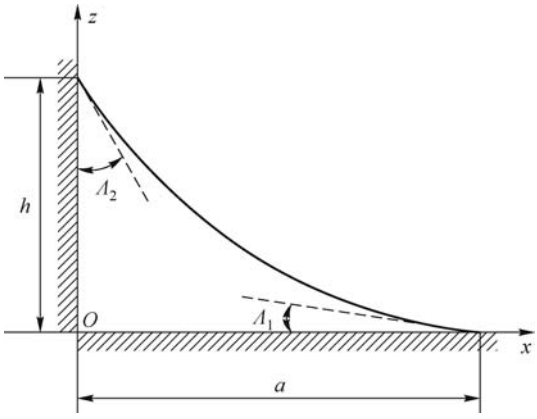

Fig. 9.5 A liquid bridge between a vertical wall and a substrate, where Λ_1 and Λ_2 are the Young's contact angles of the substrate and the side wall. respectively.

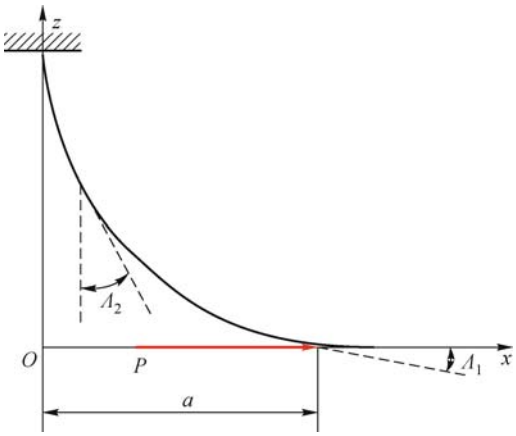

Fig. 9.6 A cantilever under a concentrated force at the free end. where Λ_1 is the slope angle at the free end. and Λ_2 is the angle between the tangent line and the vertical line at an arbitrary point.

(Table 9.1). The present analyses can make us grasp the nature of this physical phenomenon deeply and widely, and give us some inspirations to design certain analogy experiments between a meniscus and an elastica. Moreover, the calculated results are beneficial to engineering applications, such as design and fabrication of MEMS and some micro-manipulations in micro/nanotechnology.

Table 9.1 Analogies between a meniscus and a cantileve

Items	Liquid bridge or bubble	Cantilever
Governing equation	$z''(1+z'^2)^{-3/2} = c_0 + \alpha^2 z$	$z''(1+z'^2)^{-3/2} = \beta^2 z$
Stiffness	Surface tension (γ)	Bending stiffness (EI)
Generalized force	ρg or Δp	P or M
Curvature	$\Delta p/\gamma$	$M/(EI)$
Reduced parameter	$\alpha = \sqrt{\rho g/\gamma}$	$\beta = \sqrt{P/(EI)}$
Angle (Λ_1)	Young's contact angle on the substrate	Slope angle at free end
Angle (Λ_2)	Young's contact angle on the wall	Angle between the beam and the vertical line
Parameter (a)	Maximum width	Maximum deflection
Internal potential energy	Surface energy $\left(\gamma \int_0^a \sqrt{1+z'^2}\mathrm{d}x\right)$	Strain energy $\left(\frac{EI}{2}\int_0^l \varphi'^2 \mathrm{d}s\right)$
External potential energy	$-\int_0^a (\Delta p_0 + \rho g z) x z' \mathrm{d}x$	$-Pa$
Conservative parameter	Area of the meniscus S	Length of the beam l

9.4 Hierarchical structure of micro-beams induced by capillary force

In reality, the arrays of hairs, nanotubes and nanowires often form hierarchical structures as a result of capillary adhesion. The level number of structural hierarchy is dependent on the number, spacing and elasticity of hairs. Bico et al.[29] found the bundle aggregation of two bundles of hairs withdrawn from water. Based upon this investigation, Py et al.[39] found wet fibrous structures tend to self-assemble into bundles while the liquid evaporates. They studied the complex 3D aggregation process of the bundles. Furthermore, they showed that the physical process imposes a maximal size for the aggregates, which appears as the relevant scale for the distribution. Their simple toy model involving the aggregation of nearest neighbors exhibits the same statistics. The mean-field theory accounting for a maximal size is in agreement with both experiments and numerics[40].

In the real world, we can observe that the level number of structural hierarchy depends on the number, spacing and elasticity of hairs. For simplicity and without loss of generality, Liu et al.[35] considered the adhesion of $N = 2^n (n = 1, 2, 3, \cdots)$ hairs of a periodic array. They may form different structures in the case of adhesion, and the actual structure tends to minimize the total potential energy. Thus, the one-level adhesion morphology in Fig.9.7 and the hierarchical (multi-level) structures in Fig.9.8 are compared

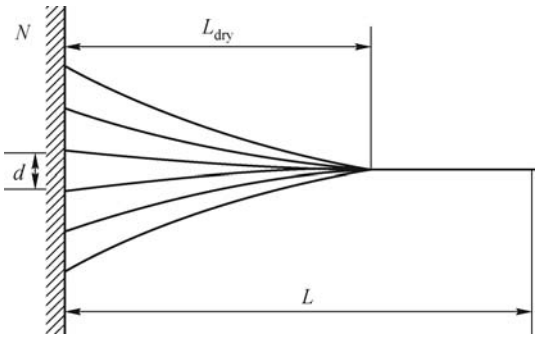

Fig. 9.7 One-level structure of a bundle of beams.

in order to find out which one is the most energetically favorable. Figure 9.8a illustrates a two-level adhesion in which any two hairs combine into a larger one and the bundled hairs will adhere further in the second level, Fig.9.8b delineates another two-level configuration in which any three hairs group in the first level, and Fig.9.8c gives a hierarchical structure in which each beam of the N level is composed of two smaller beams of the $N-1$ level. For conciseness, they give in the sequel only the energy expression of the hierarchical system in Fig.9.8c. Its non-dimensional potential energy at the equilibrium

state is written as

$$\widetilde{\Pi}_3 = A_1 B - (2^n - 1), \tag{9.8}$$

where $A_1 = (2^n - 1)\left(\dfrac{2^{2n} + 2^n}{6}\right)^{1/4}$ and $B = (3^{-3/4} + 3^{1/4})(A)^{1/4}$.

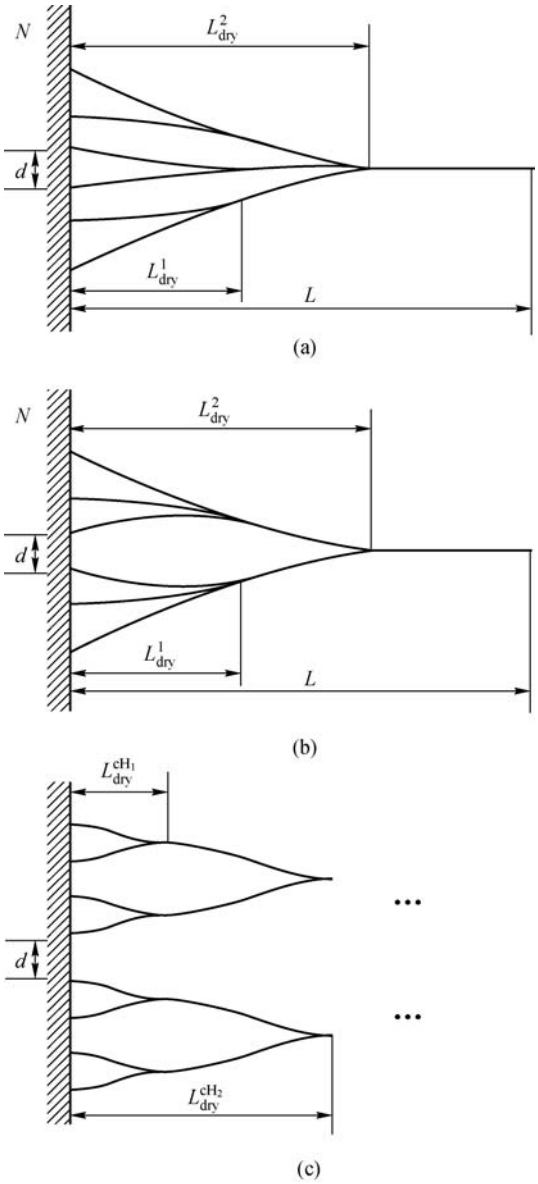

Fig. 9.8 Three possible hierarchical stnutures of a bundle of beams.

For the hierarchical structure in Fig.9.8c, the potential energy of the nth hierarchy is written as

$$\widetilde{\Pi}_{\mathrm{H}_n} = A_2 B - (2^n - 1), \tag{9.9}$$

where $A_2 = 2^{3(n-1)/4} + 2\dfrac{1 - 2^{3(n-1)/4}}{1 - 2^{3/4}}$.

The energy values of the one-level and hierarchical structures are compared in terms of the non-dimensional parameters, A_1 and A_2. It is seen that for a larger number n of hairs, the relation $A_1 > A_2$ or $\widetilde{\Pi}_3 > \widetilde{\Pi}_{\mathrm{H}_n}$ always holds, or in other words, the energy of the hierarchical structure is lower than that of the one-level structure. Therefore, the hierarchical phenomenon is more energetically favorable. This explains why the hierarchical phenomena can often be observed in reality, such as the hierarchical structure of two bundles of hairs dipped into water[29], as shown in Liu's experiment of Fig.9.9. Using the infinitesimal deformation theory of elasticity, the deflection of the adhered hairs in such a hierarchical structure can also be simulated as in Section 9.2 but it is omitted here for simplicity.

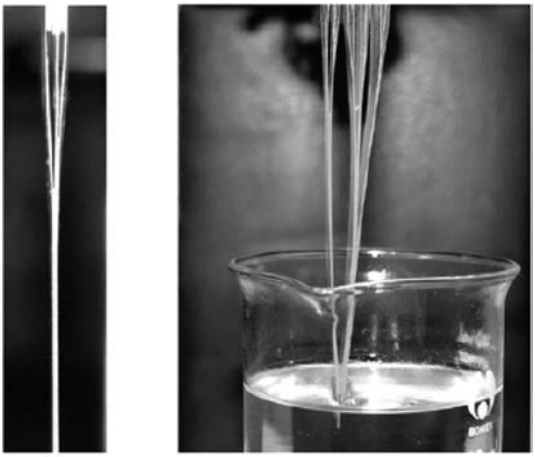

Fig. 9.9 Experimental photos for the hierarchical structures.

9.5 Capillary adhesion of a plate

In addition to the beam's stiction, there are some other micro-structures which can be adhered on the substrate due to capillary force. For instance, the stiction of a thin plate induced by the capillary force has attracted much attention to the broad range of applications, such as MEMS industry and

micro/nano- technology. Lin et al.[41] investigated the adhesion criterion between a center-anchored circular plate and its underlying substrate caused by strong capillary forces. The calculation result gives a critical gap for stiction. Bico's group[42,43] studied a paper or thin sheet wrapped by a liquid drop, which is of finite deformation state. Moreover, Liu[44] provided another novel method to calculate the capillary adhesion problem of the plate through analytical method.

The model is a thin plate with an arbitrary geometry, whose bound is clamped on a plane curve Γ_1. Refer to a Cartesian coordinate system $O-xz$, as shown in Fig.9.10. The plate is assumed to be adhered on the rigid substrate due to the capillary force induced by a liquid film between the stiction part of the plate and the substrate. Consequently, the plate includes a non-adhered part and an adhered one, denoted by D_1 and D_2, respectively. The boundary of the adhesion zone is assumed as a plane curve Γ_2 as well. The initial distance between the substrate and the plate is H, and the deflection of the plate is w. The deflection of the plate w is much smaller than the thickness of the plate, i.e. the plate is in the infinitesimal deformation state. As the thickness of the liquid film is quite thin, its total volume can be ignored in calculation, but in some cases its real morphology must be incorporated[15,33].

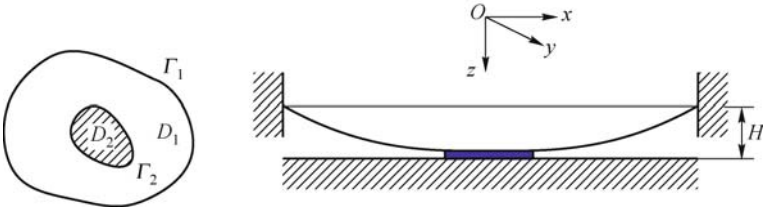

Fig. 9.10 Capillary adhesion of a micro-plate on the substrate.

In consideration of the bounds of plate being clamped fixedly on a plane curve Γ_1, the strain energy may be derived as

$$U = \frac{\kappa}{2} \iint_{D_1} (\nabla^2 w)^2 \mathrm{d}x\mathrm{d}y, \tag{9.10}$$

where the bending rigidity of the plate is $\kappa = Eh^3/[12(1-\upsilon^2)]$, h the thickness and υ the Poisson's ratio of the plate. The potential energy functional of the plate-substrate can be expressed as

$$\Pi = \iint_{D_1} F \mathrm{d}x\mathrm{d}y - 2 \iint_{D_1+D_2} \gamma \cos\theta_{\mathrm{Y}} \mathrm{d}x\mathrm{d}y, \tag{9.11}$$

where $F = F(w_{xx}, w_{yy}) = \dfrac{\kappa}{2}(\nabla^2 w)^2 + 2\gamma\cos\theta_{\mathrm{Y}}$.

Considering the moving boundary conditions and taking variation of Eq. (9.11), one can obtain the corresponding Euler – Ostrogradskii equation, that

is,

$$\nabla^4 w = 0, \quad (x, y) \in D_1. \tag{9.12}$$

During the variation process, one can get the supplementary boundary condition, i.e. the transversality condition, according to the principle of minimum total potential energy

$$\left[\frac{\kappa}{2}(\nabla^2 w)^2 + 2\gamma\cos\theta_{\mathrm{Y}} + \kappa\frac{\partial}{\partial n_2}(\nabla^2 w)\frac{\partial w}{\partial n_2} - \kappa\nabla^2 w\frac{\partial^2 w}{\partial n_2^2}\right]\Bigg|_{\Gamma_2} = 0. \tag{9.13}$$

Eq.(9.13) represents the equilibrium condition about the surface energy and strain energy on the moving bound.

Especially, the case of a circular plate adhered on the rigid substrate is investigated. For the axi-symmetrical shape of the circular plate, the stiction domain is also a circle. The initial radius of the plate is R_1, the radius of the adhered circle is R_2, and the other parameters or constraints are the same as those in Fig.9.9. In combination with Eqs.(9.12) and (9.13), one has

$$\frac{\mu}{2} = \frac{\lambda^2 - 1 - 2\ln\lambda}{(\lambda^2-1)^2 - 4\lambda^2(\ln\lambda)^2}, \tag{9.14}$$

where the non-dimensional parameter $\mu = \dfrac{R_1^2}{H}\sqrt{\dfrac{\gamma\cos\theta_{\mathrm{Y}}}{\kappa}}$. This expression indicates that μ is not a monotonic function of λ, but has a minimum value μ_{c} with the corresponding value λ_{c}. When $\lambda < \lambda_{\mathrm{c}}$, μ decreases with the increasing of λ; but when $\lambda > \lambda_{\mathrm{c}}$, μ should increase with the increasing of λ. As is well known, when the radius of the plate R_1 and the surface tension of the liquid γ increase, or the initial gap between the plate and the substrate H and the bending rigidity of the plate κ decreases, the plate can be more easily adhered on the substrate. Henceforth, the non-dimensional variable μ should increase with increasing λ. The former part of the evolution rule about μ and λ conflicts with the physical phenomenon, which is not reasonable and should be discarded.

To reduce the adhesion of the plate, the initial radius of the plate $R_1$and the surface tension of the liquid γ must be decreased, or the initial gap between the plate and the substrate H and the bending rigidity of the plate κ should be increased. Also, the stiction of the plate is related with the Young's contact angles of the plate and the substrate. To satisfy Eq.(9.14), the Young's contact angle must satisfy $\cos\theta_{\mathrm{Y}} \geqslant 0$, which indicates that only when $\theta_{\mathrm{Y}} \leqslant 90°$, i.e. the plate and the substrate are both hydrophilic, can the plate be adhered on the substrate. This provides some good advices to the electronic engineers that to avoid the adhesion of the micro-structures in MEMS, the structures and the substrate should be modified to hydrophobicity.

From Eq.(9.14), it can be seen that in order to adhere on the substrate, the radius of the plate must satisfy $R_2 \geqslant R_{\mathrm{c}} = \lambda_{\mathrm{c}} R_1$. If $R_2 < R_{\mathrm{c}}$, the

adhesion phenomenon of the plate will not occur. Minimizing μ with respect to λ yields $\mathrm{d}\mu/\mathrm{d}\lambda = 0$, i.e.

$$8\lambda^2(\ln\lambda)^3 + 8\lambda^2(\ln\lambda)^2 - 8\lambda^2(\lambda^2-1)\ln\lambda + (\lambda^2+1)(\lambda^2-1)^2 = 0. \quad (9.15)$$

The solution of Eq.(9.15) is $\lambda_c \approx 0.176$, which corresponds to the critical value $\mu_c = 8.868$. This means that the plate can not stick to the substrate at a single contact point, but takes an initial value of adhesion radius. The result of λ_c accords with the approximated result 0.175 and the experimental result 0.15[15]. The slight difference between these calculated results and the experimental result may be due to the meniscus effect of the liquid film and the nonideal boundary conditions.

Identically, the above analyses are adaptable to the solid-solid contact case, i.e. the surface energy is displaced by $-\iint\limits_{D_1+D_2} \gamma_S \mathrm{d}x\mathrm{d}y$, where γ_S is the interfacial adhesion energy of per unit contact area. In this case, the boundary conditions are the same as those of the plate-liquid-substrate contact. The dependence relationship between the detachment radius $R_d(=R_1-R_2)$ and the parameter $H^{1/2}h^{3/4}$ is

$$H^{\frac{1}{4}}h^{\frac{3}{4}} = \frac{R_d\left[12(1-\upsilon^2)\gamma_s/E\right]^{\frac{1}{4}}}{8^{\frac{1}{4}}(1-\lambda)F^{\frac{1}{2}}}, \quad (9.16)$$

where $F = F(\lambda) = (\lambda^2 - 1 - 2\ln\lambda)/[(\lambda^2-1)^2 - 4\lambda^2(\ln\lambda)^2]$. This calculated result and the experimental result[15] are compared, indicating that the two results are agreeable in tendency. The reason for the difference between the two results may be that part of the parameters are not listed in the reference, for example, the poisson's ratio of the polysilicon υ is taken as 0.23 for calculation.

9.6 Conclusions

With the development of micro/nano science and technology, it has been a hot topic for the advanced science to design and fabricate new materials and new devices in micro/nano scale. Consequently, the wetting property, deformation and self-assemble effect of micro-structures induced by capillary force must be considered properly. In this chapter, we review the capillary adhesion of micro-beams and micro-plates, which is termed part of the "elasto-capillary phenomena". Generally, all kinds of elasto-capillary phenomena can be divided into the following aspects, namely, capillary adhesion, capillary assembly, deformation or collapse induced by capillary force, and capillary buckling or wrinkling. For brevity's sake, only the capillary adhesion is discussed in this review.

We demonstrated the general theory and analysis method of capillary adhesion, dealing with the competition between the strain energy and the surface energy. Firstly, the total potential energy of the system must be constructed. Then according to the principle of minimum total potential energy, the governing equation and the transversality condition associated with the moving boundary condition are derived. The finite deformation and the hierarchical structure are also considered, mainly due to the energy equilibrium.

However, there still remain a lot of unsolved problems about capillary adhesion, such as the adhesion of a single CNT on the substrate, assembly of the CNT forest, and the problem of CNT beaten down for the existing water. Capillary effect of nano-indention, capillary assembly of the cell and biology setae are also important issues to be investigated.

These analyses may provide some inspirations for the design of micro-devices, CNT forest, MEMS, micro-sensor and non-wetting materials from different aspects (e.g., geometric shape, characteristic size, surface microstructure and elasticity).

Acknowledgements

The project was supported by the National Natural Science Foundation of China (10802099), Doctoral Fund of Ministry of Education of China (200804251520), Natural Science Foundation of Shandong Province (2009ZRA05008), Fundamental Research Funds for the Central Universities (27R0915031A).

References

[1] Neinhuis C and Barthlott W. Characterization and distribution of water-repellent, self-cleaning plant surfaces. *Ann Bot*, 79: 667-677, 1997.

[2] Otten A and Herminghaus S. How plants keep dry: a physicist's point of view. *Langmuir*, 20: 2405-2408, 2004.

[3] Liu J L, Feng X Q, Wang G F, et al. Mechanisms of superhydrophobicity on hydrophilic substrates. *J Phys: Condens Matter*, 19: 356002, 2007.

[4] Hu D L, Chan B and Bush J W M. The hydrodynamics of water strider locomotion. *Nature*, 424: 663-666, 2004.

[5] Liu J L, Feng X Q and Wang G F. Buoyant force and sinking conditions of a hydrophobic thin rod floating on water. *Phys Rev E*, 76: 066103, 2007.

[6] Stewart D. The quest to quench. *Nat Wildlife*, 42: 52-56, 2004.

[7] Hu D L and Bush J W M. Meniscus-climbing insects. *Nature*, 437: 733-736, 2005.

[8] Prakash M, Quere D and Bush J W M. Surface tension transport of prey by feeding shorebirds: the capillary ratchet. *Science*, 320: 931-934, 2008.

[9] Whitesides G M and Grzybowski B. Self-assembly at all scales. *Science*, 295: 2418-2421, 2002.

[10] Blossey R. Self-cleaning surfaces: virtual realities. *Nature Mater*, 2: 301-306, 2003.

[11] Liu J L, Xia R, Li B W, et al. Directional motion of droplets in a conical tube or on a conical fibre. *Chin Phys Lett*, 24: 3210-3213, 2007.

[12] Zhao Y P, Wang L S and Yu T X. Mechanics of adhesion in MEMS: a review. *J Adhesion Sci Technol*, 17: 519-546, 2003.

[13] Israelachvili J N. Intermolecular and Surface Forces. I2nd ed. Academic, San Diego, CA, 1992.

[14] Mastrangelo C H and Hsu C H. Mechanical stability and adhesion of microstructures under capillary forces, part I: basic theory. *J Microelectromech Syst*, 2: 33-43, 1993.

[15] Mastrangelo C H and Hsu C H. Mechanical stability and adhesion of microstructures under capillary forces, part II: experiments. *J Microelectromech Syst*, 2: 44-55, 1993.

[16] Tang T, Hui C Y and Glassmaker N J. Can a fibrillar interface be stronger and tougher than a non – fibrillar one? *J R Soc Interface*, 2: 505-516, 2005.

[17] Hui C Y, Jagota A, Lin Y Y, et al. Constraints on microcontact printing imposed by stamp deformation. *Langmuir*, 18: 1394-1407, 2002.

[18] Capovilla R and Guven J. Geometry of lipid vesicle adhesion. *Phys Rev E*, 66: 041604, 2002.

[19] Gruhn T and Lipowsky R. Temperature dependence of vesicle adhesion. *Phys Rev E*, 71: 011903, 2005.

[20] Seifert U. Dynamics of a bound membrane. *Phys. Rev. E*, 49: 3124-3127, 1994.

[21] Gorb S and Scherge M. Biological microtribology: anisotropy in frictional forces of orthopteran attachment pads reflects the ultrastructure of a highly deformable material. *Proc R Soc Lond B*, 267: 1239-1244, 2000.

[22] Geim A K, Dubonos S V, Grigorieva I V, et al. Microfabricated adhesive mimicking gecko foot-hair. *Nature Mater*, 2: 461-463, 2003.

[23] Gao H J, Wang X, Yao H M, et al. Mechanics of hierarchical adhesion structures of geckos. *Mech Mater*, 37: 275-285, 2005.

[24] Yao H M and Gao H J. Shape insensitive optimal adhesion of nanoscale fibrillar structures. *P Natl Acad Sci USA*, 101: 7851-7856, 2004.

[25] Williams J A and Le H R. Tribology and MEMS. *J Phys D: Appl Phys*, 39: R201-R214, 2006.

[26] Li Q W, DePaula R, Zhang X F, et al. Drying induced upright sliding and reorganization of carbon nanotube arrays. *Nanotechnology*, 17: 4533-4536, 2006.

[27] Wei B Q, Vajtai R, Jung Y, et al. Microfabrication technology: organized assembly of carbon nanotubes. *Nature*, 416: 495-496, 2002.

[28] Lu C H, Qi L M, Yang J H, et al. Hydrothermal growth of large-scale micropatterned arrays of ultralong ZnO nanowires and nanobelts on zinc substrate. *Chem Commun*, 33: 3551-3553, 2006.

[29] Bico J, Roman B, Moulin L, et al. Adhesion: elastocapillary coalescence in wet hair. *Nature*, 432: 690, 2004.

[30] Zhu J, Ru C Q and Mioduchowski A. Surface energy-driven adhesion of two opposing microcantilevers. *Acta Mech*, 184: 33-45, 2006.

[31] de Boer M P and Michalske T A. Accurate method for determining adhesion of cantilever beams. *J Appl Phys*, 86: 817-827, 1999.

[32] Li X and Peng Y. Investigation of capillary adhesion between the microcantilever and the substrate with electronic speckle pattern interferometry. *Appl Phys Lett*, 89: 234104, 2006.

[33] Kwon H M, Kim H Y, Puell J, et al. Equilibrium of an elastically confined liquid drop. *J Appl Phys*, 103: 093519, 2008.

[34] Kim H Y and Mahadevan L. Capillary rise between elastic sheets. *J Fluid Mech*, 548: 141-150, 2006.

[35] Liu J L, Feng X Q, Xia R, et al. Hierarchical capillary adhesion of microcantilevers or hairs. *J Phys D: Appl Phys*, 40: 5564-5570, 2007.

[36] Journet C, Moulinet S, Ybert C, et al. Contact angle measurements on superhydrophobic carbon nanotube forest: effect of fluid pressure. *Europhys Lett*, 71: 104-109, 2005.

[37] Liu J L and Feng X Q. Capillary adhesion of micro-beams: finite deformation analyses. *Chin Phys Lett*, 8: 2349-2352, 2007.

[38] Liu J L. Analogies between a meniscus and a cantilever. *Chin Phys Lett*, 26: 116803, 2009.

[39] Py C, Bastien R, Bico J, et al. 3D aggregation of wet fibers. *Europhys Lett*, 77: 44005, 2007.

[40] Boudaoud A, Bico J and Roman B. Elastocapillary coalescence: aggregation and fragmentation with a maximal size. *Phys Rev E*, 76: 060102, 2007.

[41] Lin M J and Chen R. Sticking effect on center-anchored circular plates in microstructures. *IEEE T Compon Pack T*, 24: 645-649, 2001.

[42] Py C, Reverdy P, Doppler L, et al. Capillarity induced folding of elastic sheets. *Eur Phys J Special Topics*, 166: 67-71, 2009.

[43] Py C, Reverdy P, Doppler L, et al. Capillary origami: spontaneous wrapping of a droplet with an elastic sheet. *Phys Rev Lett*, 98: 156103, 2007.

[44] Liu J L. Theoretical analysis on capillary adhesion of microsized plates with a substrate. *Acta Mechanica Sinica*, 26: 217-223, 2010.